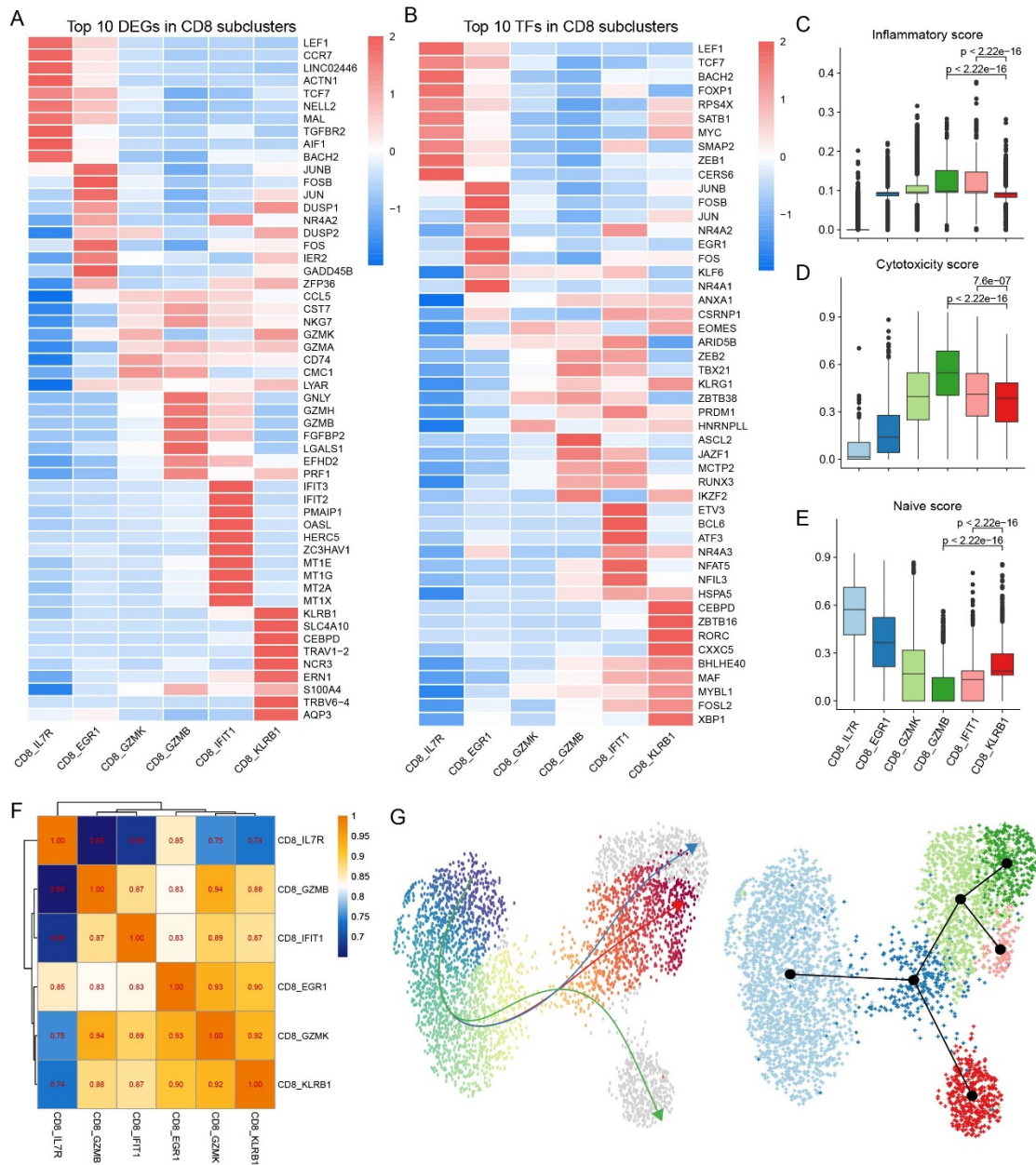


Supplemental figure 1. Single cell RNA-seq data quality control.

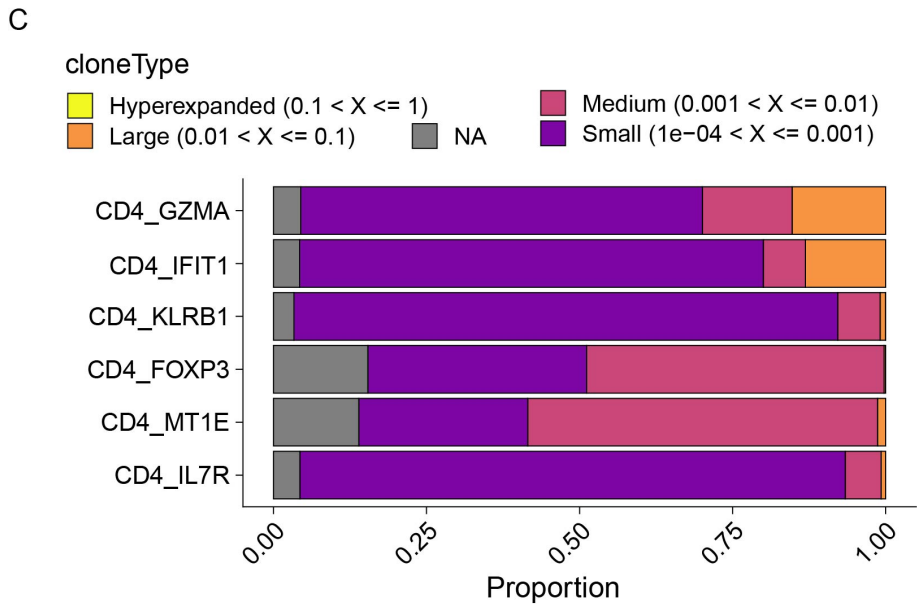
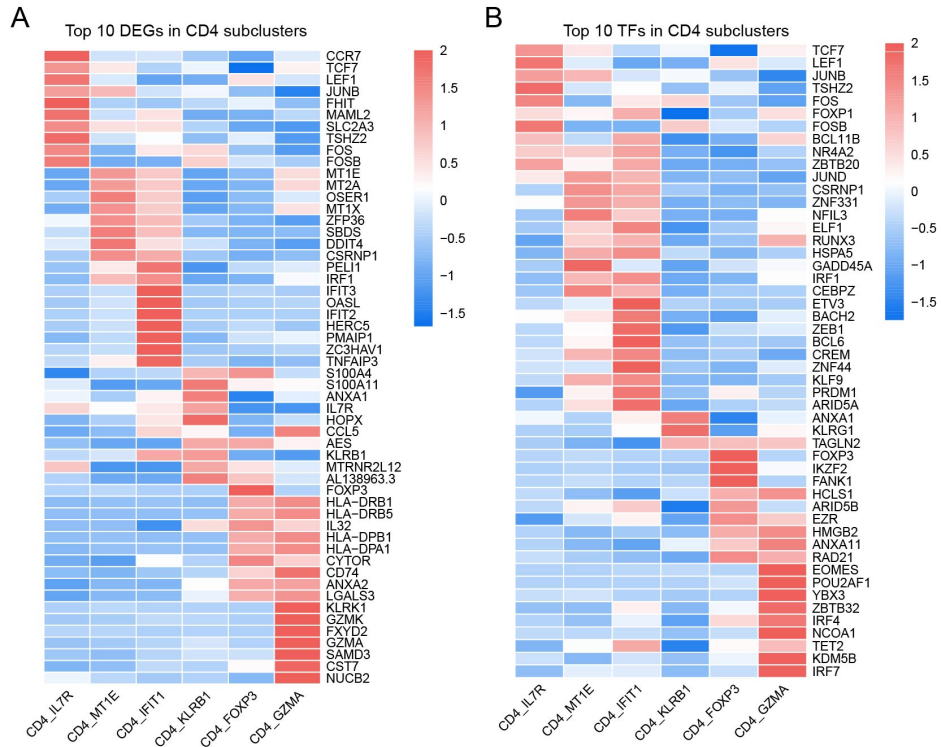
(A) The percentage of mitochondrial DNA (top panel), the number of unique molecular identifier (UMI) counts (middle panel) and genes (bottom panel) across 8 main cell clusters. (B) The percentage of mitochondrial DNA (top panel), the number of unique molecular identifier (UMI) counts (middle panel) and genes (bottom panel) across 3 sample groups. (C) The heatmap showing the expression of top 5 signature genes across 8 main cell clusters. (D) Cell distribution density across 3 sample groups. (E) The odds ratios (Ro/e) revealed the cell distribution of 8 main cell clusters across 3 sample groups using the STARTRAC-dist index method.

sample groups. (G) The odds ratios (Ro/e) revealed the cell distribution of 14 main cell clusters across 3 sample groups using the STARTRAC-dist index method. (H) Ranking of significantly differentially expressed genes among HS enriched T & NK cell and HC enriched T & NK cell. (I) GSEA plot showing pathways enriched in HS enriched T & NK cell and HC enriched T & NK cell. NES: normalized enrichment score.



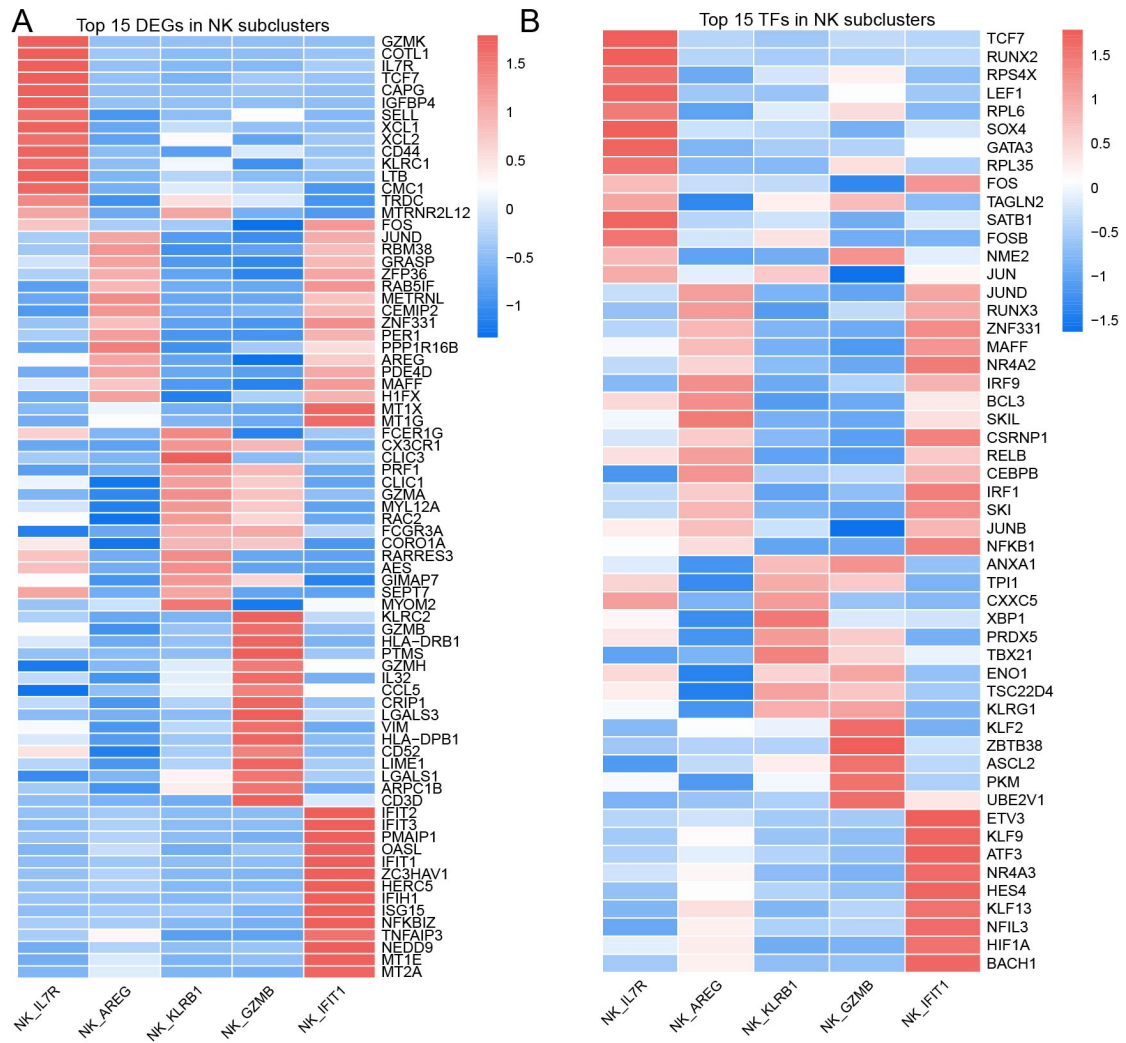
Supplemental figure 3. CD8⁺ T cell characteristics during HS onset.

(A) The heatmap showing the expression of top 10 differentially expressed genes (DEGs) across 6 CD8⁺ T cell-subclusters. (B) The heatmap showing the expression of top 10 differentially expressed transcriptome factors (TFs) across 6 CD8⁺ T cell-subclusters. (C-E) Violin plot showing the expression of T & NK cell functional signature score across 6 CD8⁺ T cell-subclusters. *P*-values were obtained using the one-way Kruskal–Wallis test followed by post-hoc Dunn’s test. (F) Heatmap showing the transcriptomic expression similarities across 6 CD8⁺ T cell-subclusters. (G) Slingshot plot showing the differentiation trajectory across 6 CD8⁺ T cell-subclusters.



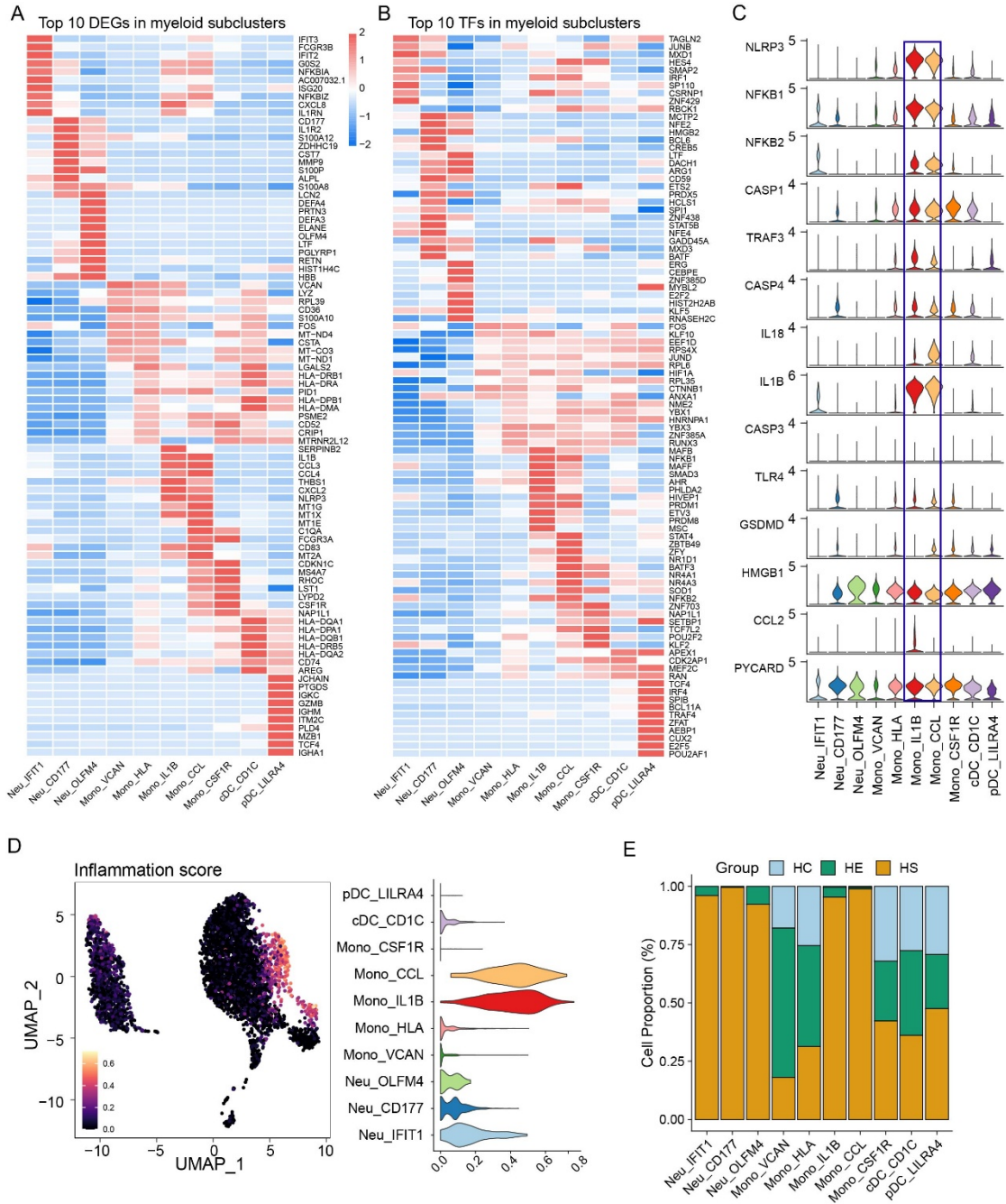
Supplemental figure 4. CD4⁺ T cell characteristics during HS onset.

(A) The heatmap showing the expression of top 10 DEGs across 6 CD4⁺ T cell-subclusters. (B) The heatmap showing the expression of top 10 TFs across 6 CD4⁺ T cell-subclusters. (C) Bar plot showing the percentage of TCR clonality types across 6 main CD4 cell-subclusters.



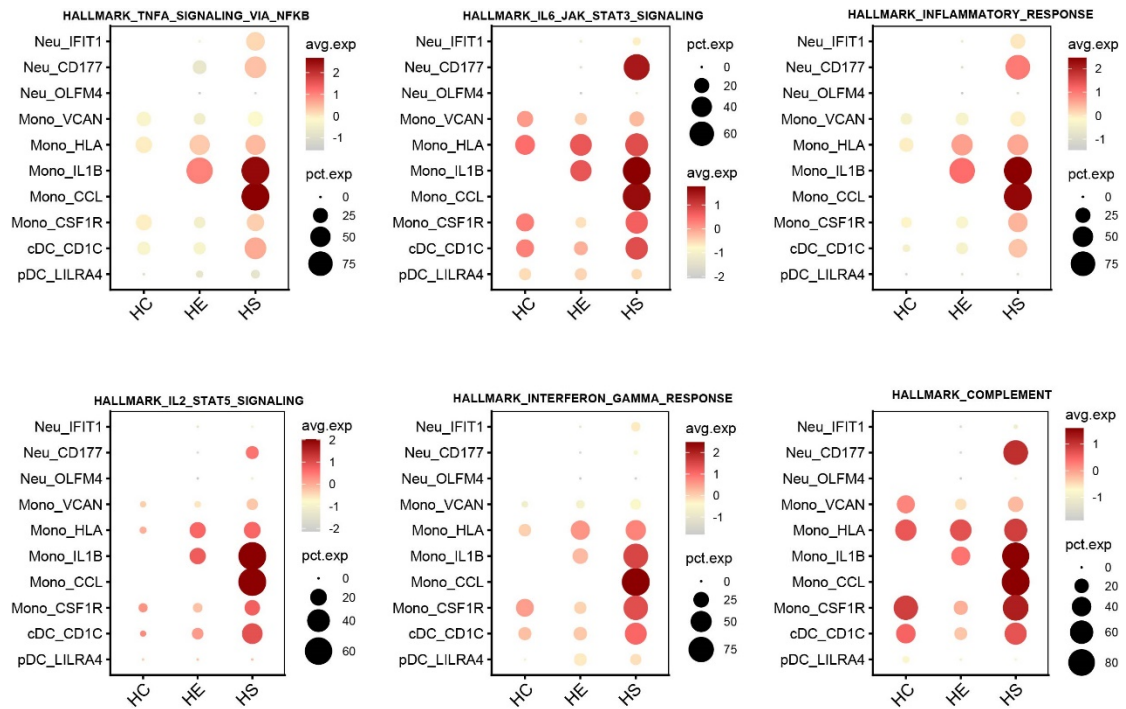
Supplemental figure 5. NK cell characteristics during HS onset.

(A) The heatmap showing the expression of top 15 DEGs across 5 NK cell-subclusters. (B) The heatmap showing the expression of top 15 TFs across 5 NK cell-subclusters.

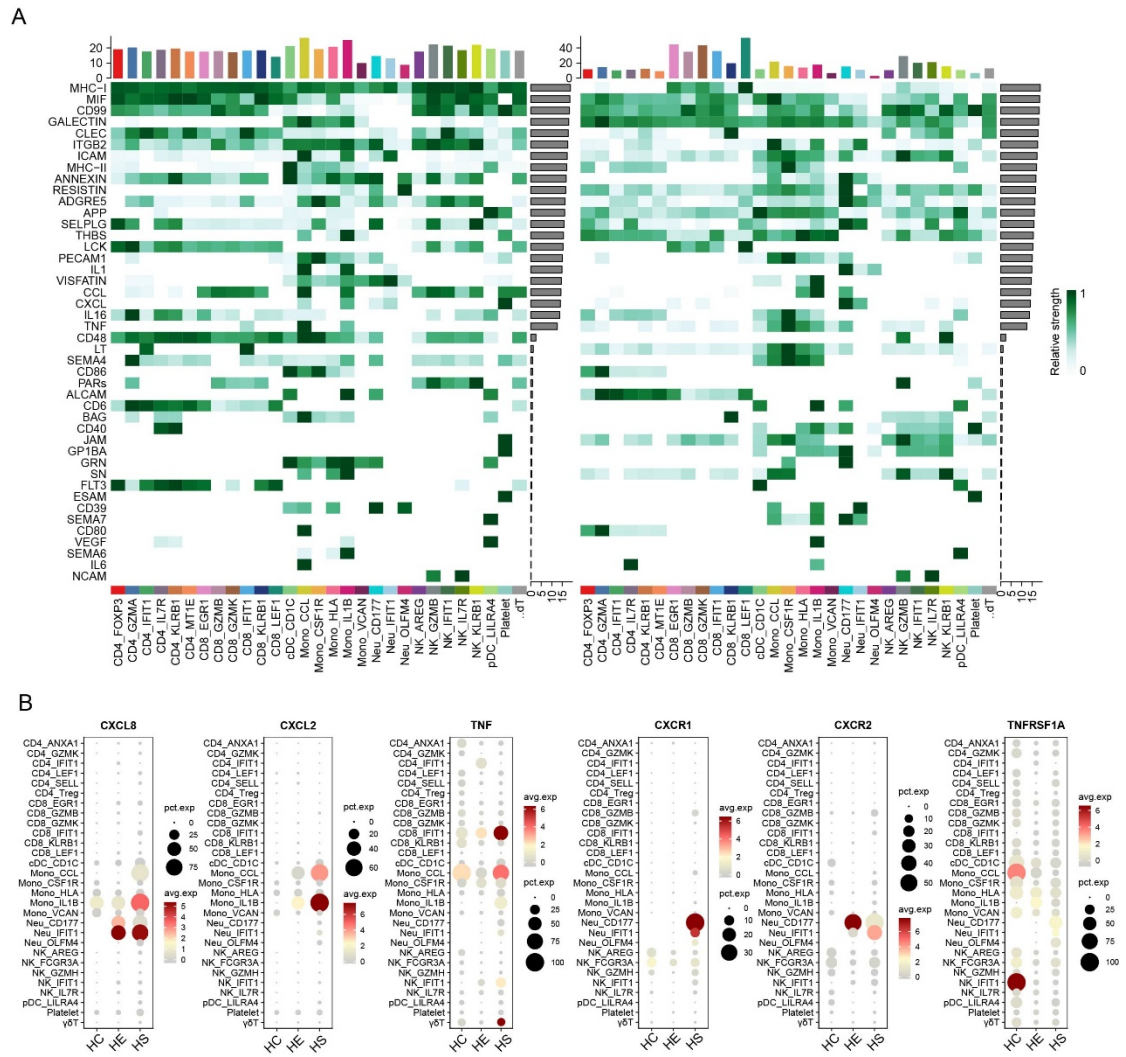


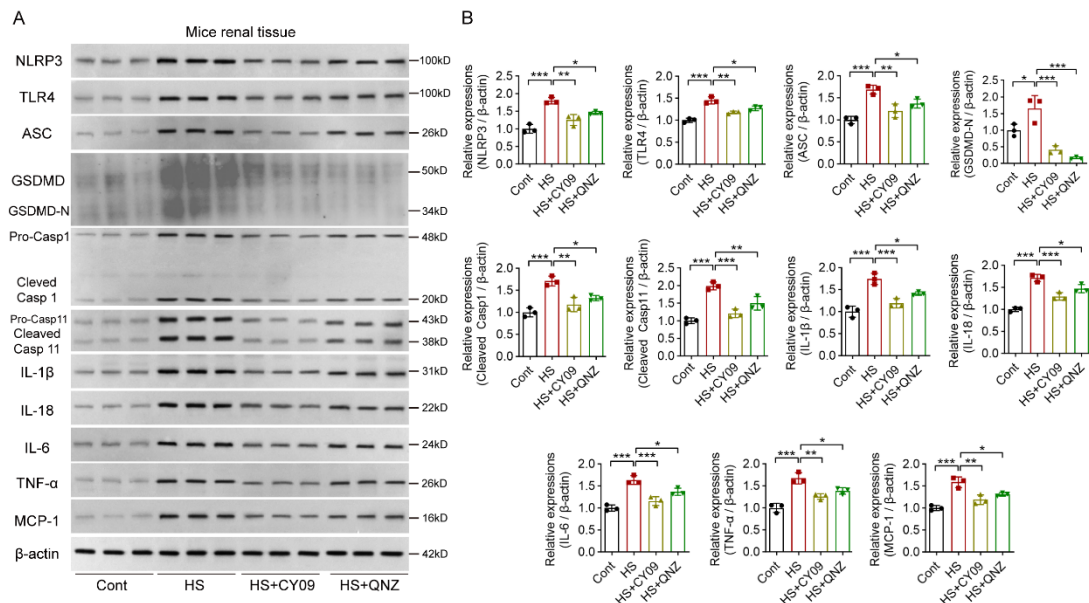
Supplemental figure 6. Myeloid cell characteristics during HS onset.

(A) The heatmap showing the expression of top 10 DEGs across 10 myeloid cell-subclusters. (B) The heatmap showing the expression of top 10 TFs across 10 myeloid cell-subclusters. (C) Stacked violin plot showing the expression of myeloid cell functional signature score across 10 myeloid cell-subclusters. (D) UMAP plot (left) and violin plot (right) showing the expression of inflammation feature score in each myeloid cell sub-cluster. (E) Barplot showing the percentage of 10 myeloid cell-subclusters in 3 sample groups.

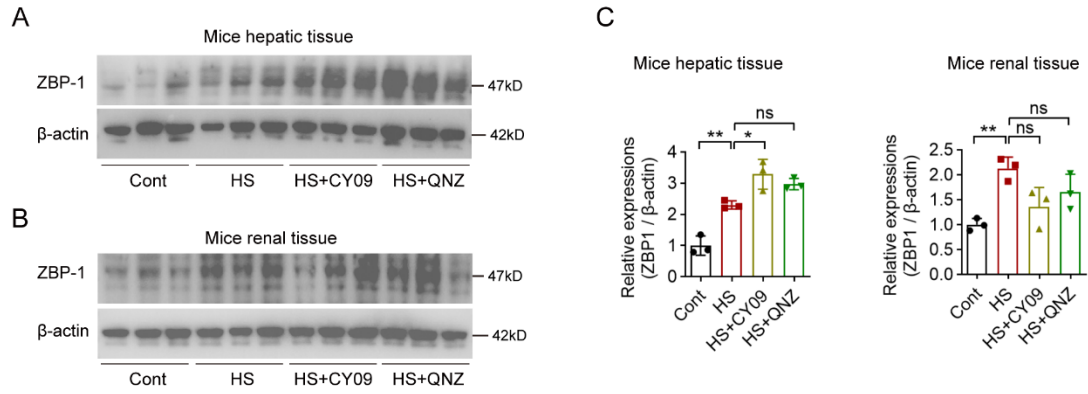


Supplemental figure 7. Myeloid cell functional characteristics during HS onset.

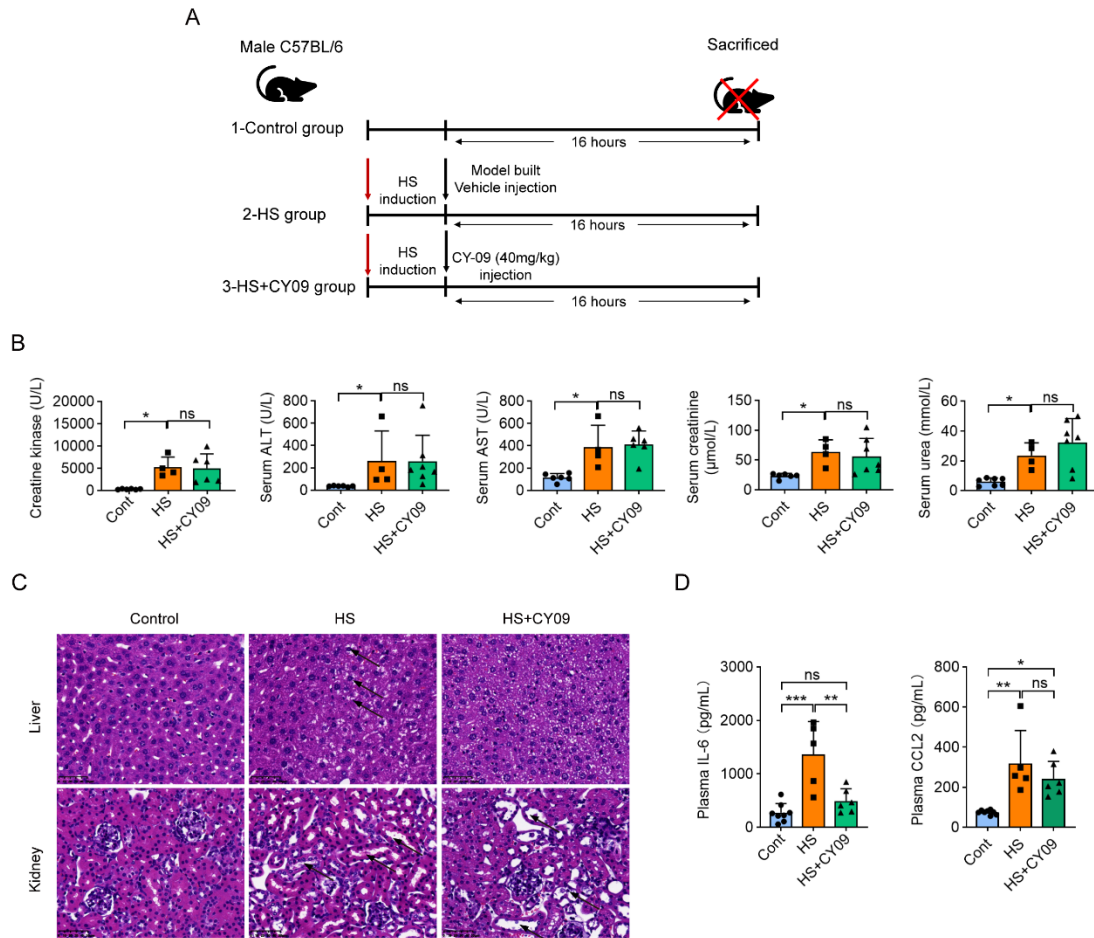




Supplemental figure 9. The expression profiles of inflammasome/pyroptosis-related proteins and inflammatory cytokines in mice renal tissues. (A) The expression profiles of inflammasome/pyroptosis-related proteins (NLRP3, TLR4, ASC, GSDMD/GSDMD-N terminal, Caspase 1, Caspase 11) and inflammatory cytokines (IL-6, IL-1 β , IL-18, TNF- α , MCP-1) in renal tissues were measured by western blotting, with β -actin as a loading control. (B) Quantitative analysis of these bands was performed and calculated for statistical significance. $n=3$ repeats per group. Comparisons were conducted using the one-way ANOVA followed by Turkey's multiple comparisons test. * $P<0.05$, ** $P<0.01$, *** $P<0.001$.



Supplemental figure 10. The expression profiles of ZBP-1 in liver and kidney tissues upon HS onset and corresponding interventions. (A and B) The expression profiles of ZBP-1 in hepatic and renal tissues were measured by western blotting, with β -actin as a loading control. (B) Quantitative analysis of these bands was performed and calculated for statistical significance. $n=3$ repeats per group. Comparisons were conducted using the one-way ANOVA followed by Turkey's multiple comparisons test. $*P<0.05$, $**P<0.01$, ns, not significant.



Supplementary figure 11. The effect of NLRP3 inhibition post HS onset on the clinical prognosis of mice. **A**, Diagram of intervention procedures for HS induction and NLRP3 inhibition. The third group was intraperitoneally injected with an NLRP3 inhibitor CY-09 (40 mg/kg) subsequently after HS induction. The second group received PBS as vehicle control. Mice were sacrificed 16 hours post-HS onset for sample collection. Serum samples were used for cytokine and biological function measurements. Hepatic and renal tissues were used for pathology staining and Western blotting. **B**, Clinical parameters measured include markers for hepatic function (ALT, AST), renal function (serum urea, creatinine), and rhabdomyolysis (creatinine kinase); $n=4\sim7$ repeats per group. **C**, Representative images of hematoxylin and eosin (H&E)-stained hepatic and renal tissues from the experimental groups. Original magnification: H&E 400X; Scale bar: 50 μm ; $n=3$ repeats per group. **D**, Plasma IL-6 and CCL2 levels in HS mice were quantified by ELISA; $n=5\sim8$ repeats per group. Comparisons were conducted using the one-way ANOVA followed by Turkey's multiple comparisons test. $*P<0.05$, $**P<0.01$, $***P<0.001$.